Med Biol Eng Comput (2016) 54:93–101
DOI 10.1007/s11517-015-1312-9

ORIGINAL ARTICLE

Does a coupling capacitor enhance the charge balance during neural stimulation? An empirical study

Marijn N. van Dongen[1] · **Wouter A. Serdijn**[1]

Received: 14 August 2014 / Accepted: 4 May 2015 / Published online: 29 May 2015

Abstract Due to their DC-blocking characteristic, coupling capacitors are widely used to prevent potentially harmful charge buildup at the electrode–tissue interface. Although the capacitors can be an effective safety measure, it often seems overlooked that coupling capacitors actually introduce an offset voltage over the electrode–tissue interface as well. This work investigates this offset voltage both analytically and experimentally. The calculations as well as the experiments using bipolar-driven platinum electrodes in a saline solution confirm that coupling capacitors introduce an offset, while they barely contribute to the passive charge balancing. In particular cases, this offset is shown to reach potentially dangerous voltage levels that could induce irreversible electrochemical reactions. This work therefore suggests that when the use of coupling capacitors is required, the offset voltage should be analyzed for all operating conditions to ensure it remains within safe boundaries.

Keywords Electric stimulation · Implantable neurostimulators · Electrodes

1 Introduction

Neural stimulation is becoming an increasingly popular clinical treatment methodology for a wide variety of diseases. In most cases, an implantable pulse generator (IPG) is used to deliver stimulation pulses to electrodes that are placed in the target area. The safety of the device is of major concern, since a faulty stimulation signal can cause irreversible damage to the neural tissue. It is especially important to prevent the flow of DCs through the electrodes [3, 7].

The use of coupling capacitors between the stimulator and the electrodes is widely considered to be an effective safety mechanism [10, 11], and indeed, various advantages concerning the use of coupling capacitors have been identified [4]. The first important advantage is the prevention of DCs in the event of device failure [9]. If, for example, one of the electrodes shorts to the supply voltage, the coupling capacitor will prevent a prolonged DC current through the electrodes.

The second important advantage that is attributed to coupling capacitors is that they improve the performance of passive charge-balancing techniques [4, 14, 15]. Charge balancing is important for polarizable electrodes to keep the electrode–tissue interface within an electrochemically safe regime [7]. A coupling capacitor helps due to its high-pass characteristics, which limits the flow of DCs, and hence, no net charge can be injected into the tissue.

A disadvantage of coupling capacitors is that their required value is often too high to be integrated on an IC [15], and hence, they are realized using bulky external components. Many studies have focused on designing stimulator output stages with accurate charge-balancing circuits [8, 13] in order to eliminate the need of coupling capacitors. Others have proposed high-frequency operation to reduce their size [5]. Indeed, the results seem to suggest that the proposed mechanisms are good enough to prevent charge accumulation on the tissue even without coupling capacitors. However, it is not clear how these systems can guarantee safety in the event of a device failure. For this reason, many stimulator systems still require the use of coupling capacitors.

✉ Marijn N. van Dongen
marijn.v.dongen@ieee.org

Wouter A. Serdijn
W.A.Serdijn@tudelft.nl

[1] Section Bio-Electronics, Delft University of Technology, Mekelweg 4, 2628CD Delft, The Netherlands

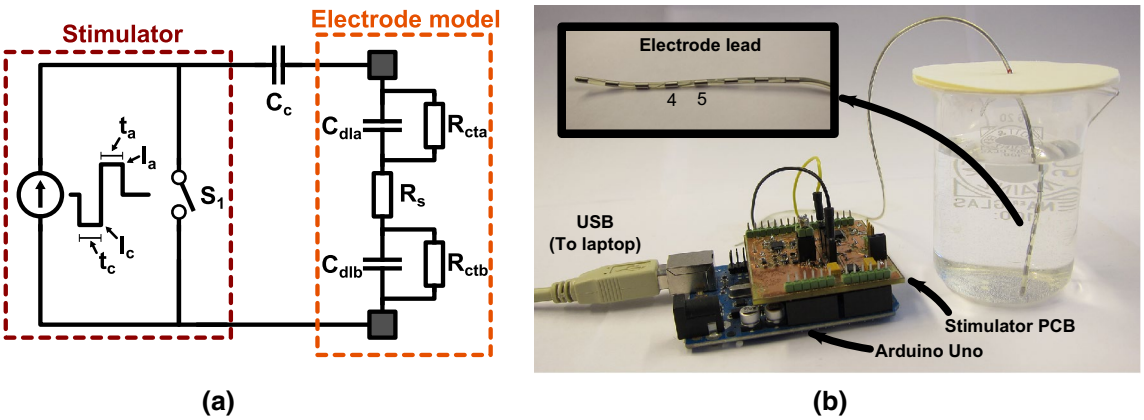

Fig. 1 **a** A basic setup of a biphasic constant current stimulator system is shown that includes a coupling capacitor C_c and an electrode model. **b** A picture of the measurement setup is shown with a detail of the electrode lead where contacts *4* and *5*, which were used for stimulation, are indicated

Although widely used, it often seems overlooked that a coupling capacitor eliminates control over the DC voltage across the electrodes. As will be shown in this work, it is therefore possible for an offset voltage V_{os} to develop over the electrode–tissue interface, even when the electrodes and capacitors are shorted in between the stimulation pulses and charge-balanced biphasic stimulation is used.

If V_{os} becomes too large, the electrode–tissue interface may leave the electrochemically safe regime, triggering the production of potentially dangerous reaction products. In this case, the intended safety mechanisms of the coupling capacitor create the opposite result: A potentially dangerous situation is created. In this work, the value of V_{os} is analyzed over various operating conditions, both analytically and experimentally. This gives insight in when V_{os} is exceeding a predefined safe regime.

2 Methods

A basic setup of a biphasic stimulator system is depicted in Fig. 1a: The coupling capacitor C_c is connected in series with the stimulator and the electrodes. The stimulation source in Fig. 1a is a biphasic constant current stimulator with a cathodic first stimulation pulse with amplitude I_c and duration t_c. The anodic charge cancelation phase follows with amplitude I_a and duration t_a. Most stimulator systems apply a passive charge-balancing scheme [15], in which the series connection of the electrodes and coupling capacitor are shorted after the stimulation cycle by closing switch S_1 to discharge C_{dl}. The duration of shorting t_{dis} is determined by the repetition rate $f_{stim} = 1/t_{stim}$ of the stimulation, since S_1 needs to be opened again when the next stimulation cycle starts.

As shown in Fig. 1a, the electrodes are modeled as a resistance R_s in series with capacitors (C_{dla} and C_{dlb}) and resistors (R_{cta} and R_{ctb}) that model the electrode–tissue interfaces of both electrodes [6]. The electrodes used in this study are single percutaneous octrode leads (manufactured by ANS, currently St. Jude Medical): They consist of eight ring-shaped platinum contacts that are distributed on a single lead. Each electrode has a diameter of 1.5 mm and a width of 3 mm (area 0.14 cm^2). A picture of the electrodes is depicted in Fig. 1b. These types of electrodes are typically used for spinal cord stimulation, and the stimulation amplitudes used in this paper are based on the specifications of the EON™ IPG (also from St. Jude Medical) [16]. The electrodes were submerged in a phosphate-buffered saline (PBS) solution containing the following: 1.059 mM KH_2PO_4, 155.172 mM NaCl, 2.966 mM Na_2HPO_4–$7H_2O$ (pH 7.4, Gibco® Life technologies™). The electrodes were connected in a bipolar fashion by selecting contacts 4 and 5 as the anode and cathode (see Fig. 1b). The other contacts were left floating.

Using an HP4194A impedance analyzer (excitation amplitude 0.1 V), it was found that for these electrodes in the PBS solution, $R_s \approx 100\ \Omega$ and $C_{dl} \approx 1.5\ \mu F$. Here, C_{dl} is the capacitive part of both electrode–tissue interfaces combined. The value of $R_{ct} \approx 1\ M\Omega$ (also combining both interfaces) was determined by measuring the voltage over the electrodes due to a 5-nA DC from a Keithley 6430 sub-femtoamp sourcemeter.

2.1 Determining V_{os}

After the anodic phase, both C_c and C_{dl} will be charged. Upon closing S_1, these capacitors will be discharged with a time constant:

$$\tau_{dis} = R_s C_{eq} \quad C_{eq} = \frac{C_c C_{dl}}{C_c + C_{dl}} \tag{1}$$

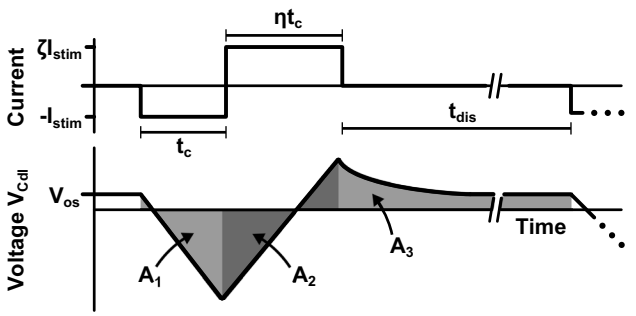

Fig. 2 Schematic plot of V_{Cdl} during a biphasic stimulation cycle with charge mismatch. When V_{os} is stable, the area $A_1 + A_2 + A_3$ equals zero

If S_1 would be closed sufficiently long, a pseudosteady state is reached in which:

$$V_{Cc} + V_{Cdl} = 0 \tag{2}$$

Here, V_{Cc} is the voltage over C_c. If S_1 is closed even longer, C_{dl} will continue to discharge through R_{ct} with time constant $\tau_2 = R_{ct}C_{dl}$ until $V_{Cdl} = 0$ V and the actual steady state is reached. However, usually $t_{dis} \ll \tau_2$, and therefore, only the pseudosteady state is reached.

Note that Eq. (2) does *not* guarantee that $V_{Cdl} = 0$ in pseudosteady state: It is an under-determined equation, and $V_{Cc} = -V_{Cdl}$ can have any value. Only when both C_c and C_{dl} are ideal capacitors, the same current is flowing through both capacitors during a stimulation cycle, which causes $V_{Cc} = V_{Cdl} = 0$ V in pseudosteady state. If these requirements are not met (e.g., when $R_{ct} \neq \infty$), the current though C_c does not equal to the current through C_{dl}, which will cause $V_{Cdl} = -V_{Cc} \neq 0$ in pseudosteady state. This charge imbalance can accumulate over many stimulation cycles, which creates an offset in V_{Cdl} [2].

We refer to Fig. 2 to analyze V_{Cdl} when after many stimulation cycles the offset voltage V_{os} is stable. In order for this voltage to be stable, the average current through R_{ct} must be zero such that no charge is lost that causes an inequality in the charge accumulated on C_{dl} with respect to C_c. Therefore, it must hold that the average value of V_{Cdl} (and hence the area as indicated in Fig. 2) is zero as well.

To find the value of V_{os} for which this requirement is met, it is assumed that the cathodic stimulation phase is characterized by a duration t_c and amplitude $I_c = I_{stim}$. In the anodic phase, both the duration $t_a = \eta t_c$ and the amplitude $I_a = \zeta I_{stim}$ can include mismatch. Furthermore, it is assumed that $t_{dis} \ll \tau_2$ (such that pseudosteady state is reached) and that R_{ct} is large enough to be neglected in the analysis (but as stated above, it must be finite). The areas A_1, A_2 and A_3 are found as:

$$A_1 = \int_0^{t_c} \left(V_{os} - \frac{I_{stim} t}{C_{dl}} \right) \mathrm{d}t = V_{os} t_c - \frac{I_{stim} t_c^2}{2C_{dl}} \tag{3a}$$

$$\begin{aligned} A_2 &= \int_0^{\eta t_c} \left(V_{os} - \frac{I_{stim} t_c}{C_{dl}} + \frac{\zeta I_{stim} t}{C_{dl}} \right) \mathrm{d}t \\ &= V_{os} \eta t_c - \frac{I_{stim} \eta t_c^2}{C_{dl}} + \frac{\zeta I_{stim} (\eta t_c)^2}{2C_{dl}} \end{aligned} \tag{3b}$$

$$\begin{aligned} A_3 &= \int_0^{t_{dis}} \left(V_{os} - (1 - \zeta\eta) \frac{I_{stim} t_c}{C_{dl}} \exp\left(\frac{-t}{R_s C_{dl}} \right) \right) \mathrm{d}t \\ &= V_{os} t_{dis} - (1 - \zeta\eta) I_{stim} t_c R_s \end{aligned} \tag{3c}$$

By setting $A_1 + A_2 + A_3 = 0$ and solving for V_{os}, the following equation is obtained:

$$V_{os} = \frac{(0.5 + \eta - 0.5\zeta\eta^2) I_{stim} t_c^2 + (1 - \zeta\eta) I_{stim} C_{dl} t_c}{C_{dl} t_c (1 + \eta) + t_{dis}} \tag{4}$$

If $\zeta = \eta = 1$, which means that perfectly charge-balanced stimulation is applied, the following equation holds:

$$V_{os} = \frac{I_{stim} t_c^2}{C_{dl}(2t_c + t_{dis})} = \frac{I_{stim} t_c^2}{C_{dl}(t_{stim})} \tag{5}$$

In Fig. 3a, the value of V_{os} is depicted for a charge-balanced stimulation cycle with $f_{stim} = 200$ Hz. This cycle includes a coupling capacitor. For small I_{stim} and t_c, the value of V_{os} is small and will have negligible influence on the system. However, for larger stimulation intensities, V_{os} starts to increase toward several hundreds of millivolts (up to 800 mV for the maximum intensity).

Equation (4) can also be used to analyze monophasic stimulation patterns by choosing $\eta = 0$. In Fig. 3b, the values of V_{os} are plotted for this situation. Somewhat surprisingly, these values are smaller than the biphasic charge-balanced stimulation. However, this can be explained by the fact that due to the relatively low value of R_s, the discharge current during t_{dis} is larger than I_{stim}, and hence, the electrodes discharge faster toward pseudosteady state as compared to the biphasic stimulation waveform.

2.2 Verifying V_{os}

To verify Eq. (4), the response of an electrode system was analyzed using both simulations and measurements in a saline bath. To simulate the response of these electrodes, the circuit from Fig. 1 was implemented in a simulator (LT-Spice). Switch S_1 was chosen to have $R_{off} = 10$ MΩ to mimic the limited output impedance of the current source and $R_{on} = 10$ Ω. The stimulation current was chosen to be $I_{stim} = 1.5$ mA ($\zeta = 1$), while an 8 % charge mismatch was introduced by making $t_c = 460$ µs and $t_a = 500$ µs ($\eta = 1.087$). After the stimulation cycle, switch S_1 was closed for $t_{dis} = 9$ ms before the next stimulation pulse is started. This makes the stimulation repetition rate slightly higher than 100 Hz.

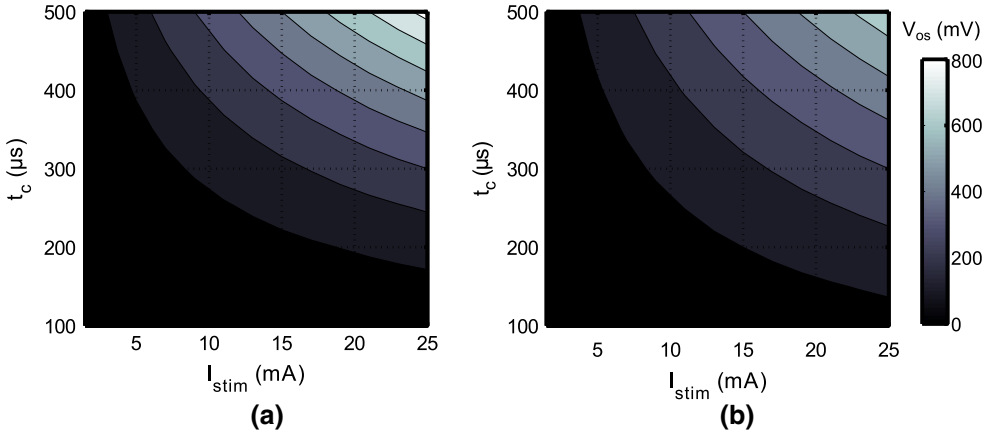

Fig. 3 Overview of the pseudosteady-state offset voltages V_{os} for a variety of stimulation settings. **a** A perfectly charge-balanced stimulation waveform is chosen, and V_{os} is determined according to Eq. (5) with $f_{stim} = 200$ Hz. **b** A monophasic stimulation waveform is used, and V_{os} is determined using Eq. (4) with $\eta = 0$

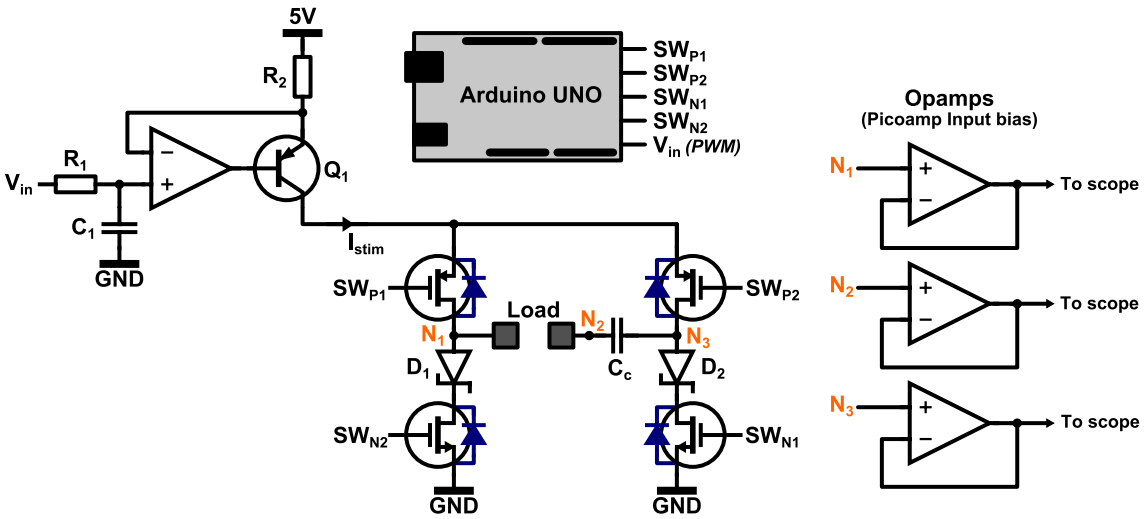

Fig. 4 Measurement setup used to verify the influence of the coupling capacitor C_c on the charge cancelation. A constant current source implemented using Q_1 is connected to the load via an H-bridge configuration (MOSFET switches), which allows bidirectional stimulation. An Arduino Uno is used for the control of the circuit, while buffers are used to prevent loading of the system during measurements

Using Eq. (1), it is found that $t_{dis} > 60\ \tau_{dis}$, which means that V_{Cdl} and V_{Cc} can be assumed to have reached their pseudosteady-state values. Also $\tau_2 = 1.5$ s $\gg \tau_{dis}$, which means that the system will stay in pseudosteady state and will not have the opportunity to fully discharge.

The value of C_c should be chosen well above C_{dl} in order to limit the contribution of C_c to the voltage headroom of the stimulator [15]. In this particular case, it was chosen to make $C_c = 8.8$ µF, based on the availability of components for the measurements. The circuit was simulated over many stimulation cycles (up to 200 s) to analyze the voltage over C_{dl} and C_c. To minimize leakage introduced by the simulation setup, the minimum conductance of the SPICE simulator was lowered from $G_{min} = 1$ pΩ^{-1} to $G_{min} = 1$ fΩ^{-1}. After a simulation, MATLAB was used to select the time stamps that correspond to pseudosteady state to obtain the values of V_{os} over many stimulation cycles.

After simulations, a stimulation circuit was built using discrete components as depicted in Fig. 4. Transistor Q_1 (2N3906) implements a current source together with resistor R_2 and the opamp (LMV358). The output current I_{stim} is controlled using the PWM signal V_{in} that is filtered using $R_1 = 1$ MΩ and $C_1 = 1$ µF. Using the H-bridge topology implemented with MOSFET devices (NTZD3155C), the current can be injected bidirectionally through the load during the cathodic and anodic stimulation phase. An Arduino

Table 1 Stimulation settings used during measurements

Nr.	Waveform	I_{stim} (mA)	t_c (μs)	Mismatch η	f_{stim} (Hz)	Incl. C_c?
1	Biphasic	1.5	460	1.085 ($t_a = 500$ μs)	110	No
2	Biphasic	1.5	460	1.085 ($t_a = 500$ μs)	110	Yes
3	Biphasic	15	200	0.75 ($t_a = 150$ μs)	400	Yes
4	Monophasic	15	200	0	100	Yes

Uno is used to control the switches: During the cathodic phase, switches SW_{P1} and SW_{N1} are closed, while during the anodic phase, switches SW_{P2} and SW_{N2} are closed. The tissue is shorted in between the stimulation pulses by closing SW_{P1} and SW_{P2}. Diodes D_1 and D_2 (CD0603–B00340) are needed to prevent unwanted current flow through the body diodes of SW_{N1} and SW_{N2}: If C_{dl} is charged beyond 0.6 V during the cathodic phase, the body diodes of SW_{N1} and SW_{N2} otherwise become forward biased when the stimulation direction is reversed.

The Arduino was programmed with four different stimulation settings as summarized in Table 1. The first setup uses no coupling capacitor, and it is verified that C_{dl} is indeed charged back to 0 V after a stimulation cycle. The second setup uses a low-intensity stimulation cycle with a positive charge mismatch, while the third setup uses a high-intensity stimulation cycle (close to the maximum stimulation intensity possible before the current source would clip to the 5 V supply voltage). The fourth experiment uses a monophasic stimulation waveform. All measurements were taken after stimulation was enabled sufficiently long (at least 5 min) to allow the voltages to settle.

The load of the circuit in Fig. 4 first consisted of the electrode model from Fig. 1 ($R_s = 100\ \Omega$, $C_{dl} = 1.5\ \mu F$, $R_{ct} = 1\ M\Omega$). Subsequently, the electrode model was replaced by the electrodes that were submerged in the PBS solution.

To measure the response of the system, the relevant output signals are buffered using picoampere input bias operational amplifiers (AD8625, powered with ±8 V) in order to prevent the measurement equipment from loading the system. It was found using simulations and measurements that a 10 MΩ ||12 pF standard probe largely distorts the measurement, as will be discussed further in the last section.

3 Results

Figure 5 shows the simulation results of the circuit from Fig. 1. In Fig. 5a, the value of V_{Cdl} in pseudosteady state is shown over many stimulation cycles. When no coupling capacitor is used, V_{Cdl} can discharge almost completely. When C_c is added in Fig. 5a, it is seen that after several stimulation cycles, $V_{Cdl} = 20.7$ mV. Indeed, the introduction of C_c causes an offset in V_{Cdl} in pseudosteady state. Furthermore, the simulated values correspond well with Eq. 4, which predicts $V_{os} = 20.6$ mV.

In Fig. 5b, c, the simulated transient behavior of the voltages in the circuit including C_c is shown for two time instances. Figure 5b shows the voltages right after the first stimulation cycle, while Fig. 5c shows the voltages during a stimulation cycle after 190 s of simulation time, where the offset is clearly visible.

In Fig. 6, the measurement results are presented for all experiments listed in Table 1. In all figures, V_{out} refers to the voltage measured over the output of the current source (between nodes N_1 and N_3 in Fig. 3) and V_{el} is the voltage over the electrode (nodes N_1 and N_2). For saline measurements, it is not possible to measure V_{Cdl} directly, and hence, V_{el} is shown instead.

4 Discussion

The measured values for V_{os} are summarized in Table 2 and compared with the values calculated using Eq. (4). It is seen that the measurements with the model correspond well to the calculated values, indicating that the circuit implementation is working as expected. For the saline measurements, the values of V_{os} are higher than expected, and hence, the model underestimates the offset value introduced. This is most likely due to complex nonlinear behavior of the electrode–tissue interface that cannot be modeled using the simple capacitance C_{dl}. The electrode model is a small-signal model (C_{dl} was found using a sinusoidal excitation of 0.1 V), and the measurement results show that the validity of the model is limited during a stimulation cycle. From these results and the plots in Fig. 6, we can draw three important conclusions.

1 First of all, coupling capacitors barely improve the way in which V_{Cdl} returns to equilibrium. The only way in which C_c contributes is by making τ_{dis} (Eq. 1) smaller during the t_{dis} interval [4]. This causes the interface to discharge toward equilibrium slightly faster. However, since $C_c \gg C_{dl}$, the influence on τ_{dis} is negligible, and hence, coupling capacitors barely improve the charge cancelation.
2 Second of all, coupling capacitors introduce an offset in the pseudosteady-state value of the electrodes. The

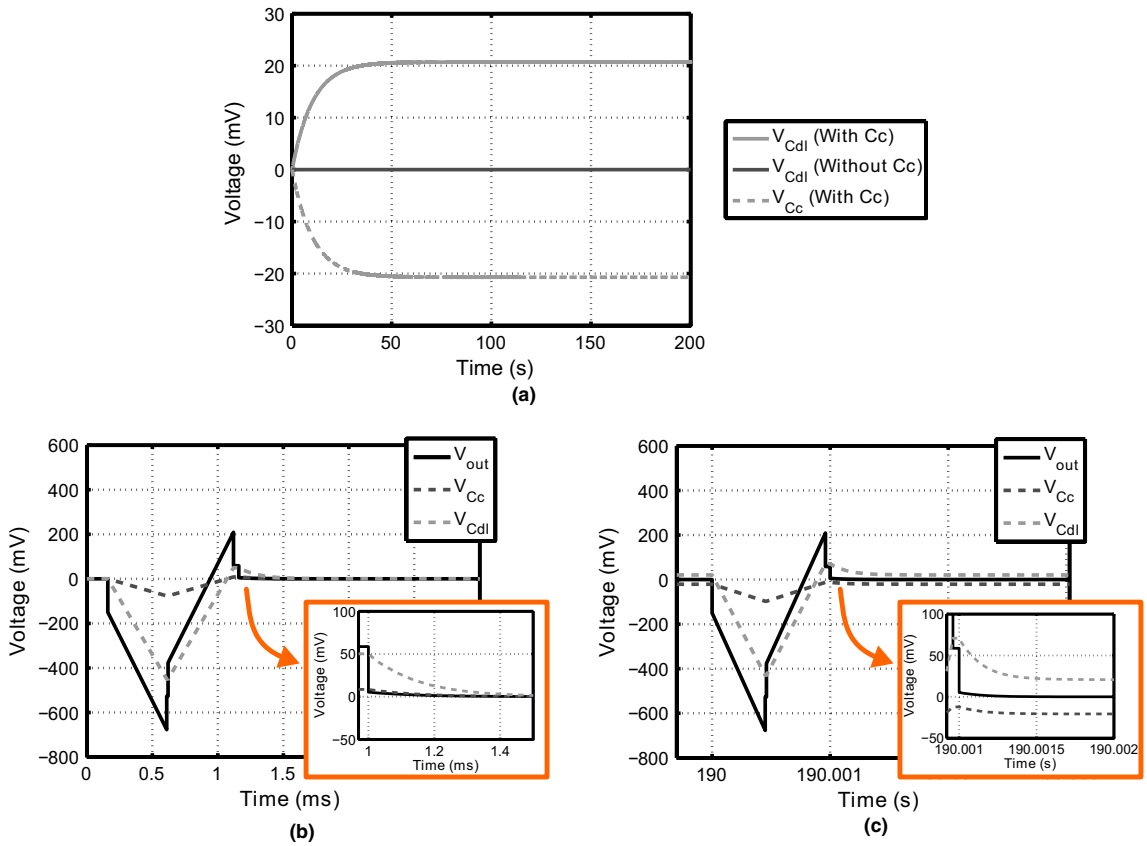

Fig. 5 Simulation results of the circuit from Fig. 1. **a** The voltages V_{Cdl} and V_{Cc} are shown during the interval t_{open} over a large number of stimulation cycles. As can be seen, the coupling capacitor causes an offset. **b**, **c** The transient voltages are shown for the system with C_c and $R_p = \infty$ just after stimulation is initiated and after 190 s, respectively

value of V_{os} can be predicted using Eq. (4), although it was found that this equation underestimated the offset measured from the electrodes in saline.

The question is whether or not V_{os} introduces potential safety issues. For small values of V_{os}, no problems are likely to occur: As long as no irreversible faradaic reactions are triggered, no harmful effects are to be expected. Even more so, V_{os} will increase the amount of charge that can be injected [1], because V_{os} reduces the peak voltage of V_{Cdl} during a stimulation cycle.

However, when V_{os} increases toward the threshold of irreversible faradaic reactions (600–900 mV for platinum electrodes [12]), problems can be expected. In this case, the interface is experiencing a significant offset voltage during the t_{dis} interval, during which irreversible reactions might occur. For high stimulation intensities, Fig. 3 predicts values of V_{os} that are close to or exceed the maximum safe voltage window.

3 Finally, secondary effects can have a strong effect on V_{os}. Using the settings of experiment 2, measurements were repeated with both the model and the electrodes as load. This time, the voltages were not buffered using the picoampere input bias opamps, but 10 MΩ ‖12 pF probes (referenced to ground) were connected to N_1, N_2 and N_3 directly. This has a large impact on the offset voltage: It increases from 25 mV to 2 V (model) and from 80 mV to 0.6 V (saline).

All in all, it can be concluded that in contrast to what many other studies have suggested [4, 14, 15], the introduction of C_c does not improve the charge-balancing process and it is furthermore associated with the loss of control over the pseudosteady-state value of V_{Cdl}. Instead of ensuring safety by returning the electrode interface voltage back to 0 V, the coupling capacitor introduces an unwanted offset in the interface voltage that is hard to control by the stimulator and, moreover, is sensitive to secondary effects.

Although this work suggests that coupling capacitors are not beneficial for charge cancelation purposes, they still protect the electrodes and tissue from DCs in case of a device or software failure. Depending on the application, this could require the need to still use these capacitors. In

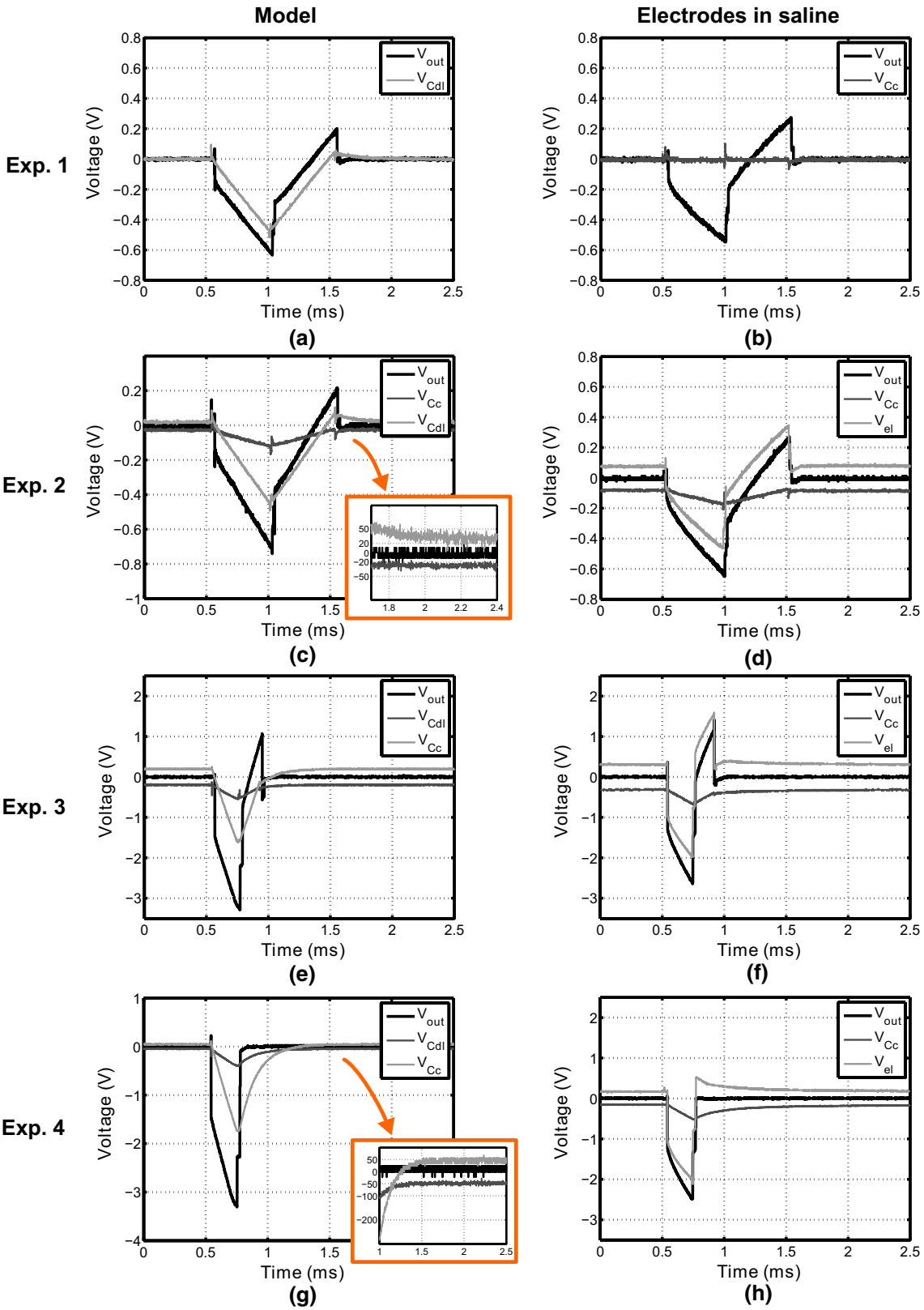

Fig. 6 Measurement results from the experimental setup depicted in Fig. 4 with the load consisting of the electrode model (*left column*) and the electrodes in saline (*right column*). For both loads, four stimulation settings are used as described in Table 1. As can be seen, the offset voltage depends on the stimulation settings used, but is zero when no coupling capacitor is used (experiment 1)

Table 2 Calculated and measured values of V_{os} for the experiments summarized in Table 1

Experiment	Equation (4) (mV)	Measurement (model) (mV)	Measurement (saline) (mV)
1	0	0	0
2	21.6	25	80
3	201	200	320
4	50	50	165

that case, the results from this study show that the stimulation settings should be limited to ensure that under all operating conditions, V_{os} does not exceed any predefined safety window.

It is possible to discharge both C_c and C_{dl} completely by introducing an additional switch over C_c. In this case, C_c and C_{dl} are shorted individually and are guaranteed to discharge toward 0 V in pseudosteady state, which would eliminate the offset. However, in this case, it is unclear how the coupling capacitor is contributing to the charge-balancing process: It does not improve τ_{dis} and V_{Cdl} will have the same response as compared to the circuit without C_c. Furthermore, the additional switch introduces a single-fault device failure risk. Therefore, the advantages of a coupling capacitor are not exploited when C_c is discharged separately.

This work focused on passive charge-balancing techniques. Active charge-balancing techniques use feedback to bring the electrode voltage back to safe values after a stimulation cycle [15] and can therefore help to overcome the offset problem. However, if these schemes require a coupling capacitor to protect in the event of a device failure, it is important to measure the voltage over the electrodes only and not to include the coupling capacitor. This requires an additional sensing pin if the coupling capacitors are realized using external components. Only then, the feedback mechanism will help to remove the offset.

In this study, only one type of electrode was considered. Smaller electrodes have different impedance levels, and more research is needed to find the pseudosteady-state response in this case. Note that Eq. (4) is only valid under the assumption that $\tau_{dis} \gg t_{dis}$, which might not be the case for high impedance electrodes. Finally, it would also be interesting to determine the influence of the coupling capacitors in vivo.

5 Conclusions

In this work, the influence of coupling capacitors on the charge-balancing properties is studied during neural stimulation. In contrast to what previous work suggests, coupling capacitors were found not to improve the charge-balancing process. Even more so, they introduce an offset voltage in the electrodes, which cannot be removed by conventional means such as passive discharging. The value of the offset voltage depends on the stimulation and electrode parameters. When using coupling capacitors, it is therefore important to ensure that this offset voltage does not exceed any safety boundaries for all possible operating conditions.

References

1. de Donaldson NN, Donaldson PEK (1986) When are actively balanced biphasic ('Lilly') stimulating pulses necessary in a neurological prosthesis? II pH changes; noxious products; electrode corrosion; discussion. Med Biol Eng Comput 24(1):50–56
2. de Donaldson NN, Donaldson PEK (1986) When are actively balanced biphasic ('Lilly') stimulating pulses necessary in a neurological prosthesis? I historical background; Pt resting potential; Q studies. Med Biol Eng Comput 24(1):41–49
3. Lilly JC, Hughes JR (1955) Brief, noninjurious electric waveform for stimulation of the brain. Science 121:468–469
4. Liu X, Demosthenous A, Donaldson N (2008) Five valuable functions of blocking capacitors in stimulators. In: Proceedings of the 13th annual international conference of the FES society (IFESS08), Freiburg, pp 322–324
5. Liu X, Demosthenous A, Donaldson N (2008) An integrated implantable stimulator that is fail-safe without off-chip blocking-capacitors. IEEE Trans Biomed Circuit Syst 2(3):231–244
6. Malmivuo J, Plonsey R (1995) Bioelectromagnetism: principles and applications of bioelectric and biomagnetic fields. Oxford University Press, New York
7. Merrill DR, Bikson M, Jeffreys JGR (2005) Electrical stimulation of excitable tissue: design of efficacious and safe stimulation protocols. J Neurosci Method 141:171–198
8. Nag S, Jia X, Thakor NV, Sharma D (2013) Flexible charge balanced stimulator with 5.6 fC accuracy for 140 nC injections. IEEE Trans Biomed Circuit Syst 7(3):266–275
9. Nonclercq A, Lonys L, Vanhoestenberghe A, Demosthenous A, Donaldson N (2012) Safety of multi-channel stimulation implants: a single blocking capacitor per channel is not sufficient after single-fault failure. Med Biol Eng Comput 50(4):403–410
10. Parramon J, Nimmagadda K, Feldman E, He Y (2013) Multi-electrode implantable stimulator device with a single current patch decoupling capacitor. US Patent 8,369,963
11. Prutchi D, Norris M (2005) Chapter 7 in design and development of medical electronic instrumentation: a practical perspective of the design, construction and test of medical devices. Wiley, New Jersey
12. Rose TL, Robblee LS (1990) Electrical stimulation with Pt electrodes VIII electrochemically safe charge injection limits with 0.2 ms pulses. IEEE Trans Biomed Eng 37:1118–1120

13. Sit J, Sarpeshkar R (2007) A low-power blocking-capacitor-free charge-balanced electrode-stimulator chip with less than 6 nA DC error for 1-mA full-scale stimulation. IEEE Trans Biomed Circuit Syst 1(3):172–183
14. Sooksood K, Stieglitz T, Ortmanns M (2009) An experimental study on passive charge balancing. Adv Radio Sci 7:197–200
15. Sooksood K, Stieglitz T, Ortmanns M (2010) An active approach for charge balancing in functional electrical stimulation. IEEE Trans Biomed Circuit Syst 4:162–170
16. St. Jude Medical Inc (2014) Eon Rechargeable IPG tech specs. http://professional.sjm.com/products/neuro/scs/generators/eon-rechargeable-ipg